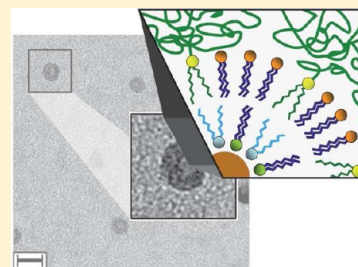


Self-Assembly of Stable Monomolecular Nucleic Acid Lipid Particles with a Size of 30 nm

Sophia Rudolf[†] and Joachim O. Rädler*[‡]

Ludwig-Maximilians-University, Geschwister-Scholl-Platz 1, D-80539 Munich, Germany

ABSTRACT: The design of efficient nucleic acid complexes is key to progress in genetic research and therapies based on RNA interference. For optimal transport within tissue and across extracellular barriers, nucleic acid carriers need to be small and stable. In this Article, we prepare and characterize mono-nucleic acid lipid particles (mono-NALPs). The particles consist of single short double-stranded oligonucleotides or single siRNA molecules each encapsulated within a closed shell of a cationic-zwitterionic lipid bilayer, furnished with an outer polyethylene glycol (PEG) shield. The particles self-assemble by solvent exchange from a solution containing nucleic acid mixed with the four lipid components DOTAP, DOPE, DOPC, and DSPE-PEG(2000). Using fluorescence correlation spectroscopy, we monitor the formation of mono-NALPs from short double-stranded oligonucleotides or siRNA and lipids into monodisperse particles of approximately 30 nm in diameter. Small angle neutron and X-ray scattering and transmission electron microscopy experiments substantiate a micelle-like core-shell structure of the particles. The PEGylated lipid shell protects the nucleic acid core against degradation by nucleases, sterically stabilizes the mono-NALPs against disassembly in collagen networks, and prevents nonspecific binding to cells. Hence, PEG-lipid shielded mono-NALPs are the smallest stable siRNA lipid system possible and may provide a structural design to be built upon for the development of novel nucleic acid delivery systems with enhanced biodistribution in vivo.



1. INTRODUCTION

The molecular design of nucleic acid delivery systems governs their functionality with regards to biodistribution, protection of the nucleic acid load, specific targeting, intracellular release, and therapeutic efficiency. Most novel delivery constructs are developed and tested in vitro. At a later stage, in vivo studies are performed that aim for improved efficiency, but are often hampered by limited transport of the construct in complex fluids or tissue. Complexation of nucleic acid with lipid is one possible route to build delivery vehicles. The discovery of cationic lipid-mediated transfection marked a breakthrough in lipid-based nonviral delivery¹ and led to commercialized applications in high-throughput screening techniques in vitro.² The cationic lipid serves to complex nucleic acid into partially ordered lipid-DNA complexes,^{3,4} which allow uptake and intracellular release.⁵ Yet cationic lipids show limited efficacy in vivo,⁶ mainly because size, morphology, and surface architecture of lipoplexes are kinetically controlled and not well tailored to meet conditions in the extracellular space. With the advent of RNA interference, the focus of nucleic acid delivery has shifted from plasmid DNA toward rather short segments of ds-RNA or ds-DNA.^{7,8} In this context, the cationic lipid condensation strategy has been reconsidered.⁶ Various carrier systems have been developed specifically for siRNA delivery, including lipid-based complexes such as genospheres^{9,10} or stable nucleic acid lipid particles (SNALPs),^{11,12} both prepared by solvent exchange. Entirely novel lipid-like materials (lipidoids) were generated by a large-scale combinatorial synthesis approach and screened with regard to silencing efficiency and toxicity.¹³ Compounds eligible for in vivo delivery were subsequently further refined with respect to

surface charge, size, and in vivo efficacy.¹⁴ Recently, it was shown that siRNA complexed with multivalent cationic lipids forms cubic phases with profound effect on the fusogenic and overall delivery efficiency.^{15,16} Still, siRNA delivery in vivo is challenging due to a multitude of systemic barriers,¹⁷ whereof many are size related. Examples are size-restricted diffusion in solid tumors and in the extracellular matrix, the effect of enhanced permeation and retention in inflamed or tumor tissue, size-related elimination by the reticuloendothelial system, limiting fenestrae of capillaries, and the size-selectivity of the blood-brain barrier.^{6,14,18,19} Hence, decreasing the size of the gene carrier can increase its in vivo efficacy. This leads us to the fundamental question: What is the smallest possible lipid-based carrier for short ds-RNA or ds-DNA? Obviously, the smallest carrier would contain only a single nucleic acid molecule, and we will denote such systems monomolecular carriers. In the literature, some attempts to assemble monomolecular gene carriers can be found. Blessing et al. described a template directed chemical synthesis of single plasmid DNA nanoparticles with a diameter of 23 nm,²⁰ a method that was extended to polymeric lipid DNA particles by Chittimalla et al.²¹ In our own work, we used block copolymers to encapsulate monomolecular siRNA or short DNA fragments, resulting in 2 nm-sized particles.^{22,23} Furthermore, the possibility of single DNA strands being enwrapped by a cationic lipid bilayer had been discussed because TEM images provided some evidence of tubular structures connected to DNA lipid particles referred to as “spaghetti”-like objects.^{24,25}

Received: April 2, 2012

Published: June 13, 2012

May et al. demonstrated theoretically that the coating of DNA by a symmetric bilayer is energetically unfavorable as compared to the bulk hexagonal phase due to high positive curvature of the outer monolayer.²⁶ Tresset et al. explored the morphologies of lipid-coated polyelectrolytes in general, and detailed X-ray studies were carried out on lipid-coated microtubules.^{27,28} However, lipid bilayer coating of individual siRNA molecules has not yet been reported.

In this Article, we show that the encapsulation of single siRNA molecules by an asymmetric cationic–zwitterionic lipid bilayer can be achieved via a solvent exchange method. We call these complexes monomolecular nucleic acid lipid particles (mono-NALPs). They are stable, monodisperse, and 30 nm in size, protect nucleic acid against nucleases, and diffuse freely in dense extracellular biopolymer solutions. Mono-NALPs are the smallest PEGylated and lipid bilayer-coated siRNA constructs possible and will serve as a design basis for novel classes of carrier systems with improved in vivo efficacy.

2. RESULTS AND DISCUSSION

2.1. Rational Design Considerations. The rationale of our mono-NALP constructs builds upon the following observations: In the early structural work on DNA lipid particles, it was shown that mixtures of DNA, cationic lipids (DOTAP, 1,2-dioleoyl-3-trimethylammonium-propane), and neutral lipids (DOPE, 1,2-dioleoyl-*sn*-glycero-3-phosphoethanolamine) form an inverted hexagonal phase H_{II}^C in a narrow concentration regime.²⁹ The structure consists of hexagonally packed lipid monolayer-coated DNA molecules. To isolate a monolayer-coated DNA in aqueous environments, it needs to be covered by a second layer. In case of an asymmetric cationic lipid bilayer, a single highly curved membrane can be stabilized by a single molecule of double-stranded nucleic acid.

Figure 1 schematically depicts the structure of a mono-NALP consisting of a single siRNA molecule enwrapped by an asymmetric lipid bilayer. The inner monolayer is rich in cationic lipid DOTAP and neutral DOPE, which exhibits negative spontaneous curvature. The outer monolayer is composed of neutral DOPC (1,2-dioleoyl-*sn*-glycero-3-phosphocholine) and a PEGylated DSPE moiety as used in stealth liposomes.

In the following, we aim to find an assembly pathway for this theoretical construct. The complexity of this problem can be reduced by considering the hierarchy of the predominant interactions. In case of particles composed of DNA or siRNA and lipids, the formation is primarily driven by electrostatic and hydrophobic interactions. At physiological conditions, DNA and siRNA carry two negative charges per base pair. Cationic lipids bind to the nucleic acid, and the monolayer is completed by the incorporation of DOPE,²⁹ as these neutral lipids have a small negative radius of spontaneous curvature of -3 nm.³⁰ In aqueous environments, this first, inverted monolayer is covered by a second lipid layer due to hydrophobicity of the lipid tails. The distal monolayer has a positive curvature and therefore requires the availability of lipids with an intrinsic curvature close to or greater than zero, like the neutral DOPC.³⁰ DSPE-PEG(2000) (1,2-distearoyl-*sn*-glycero-3-phosphoethanolamine-*N*-[(polyethylene glycol)-2000]) can be treated as a lipid with a high positive radius of spontaneous curvature (3 nm) due to a PEG chain of 45 repeat units covalently attached to the headgroup.³¹ Hence, embedding DSPE-PEG(2000) into the DOPC layer increases and thereby optimizes the spontaneous curvature of the distal monolayer.

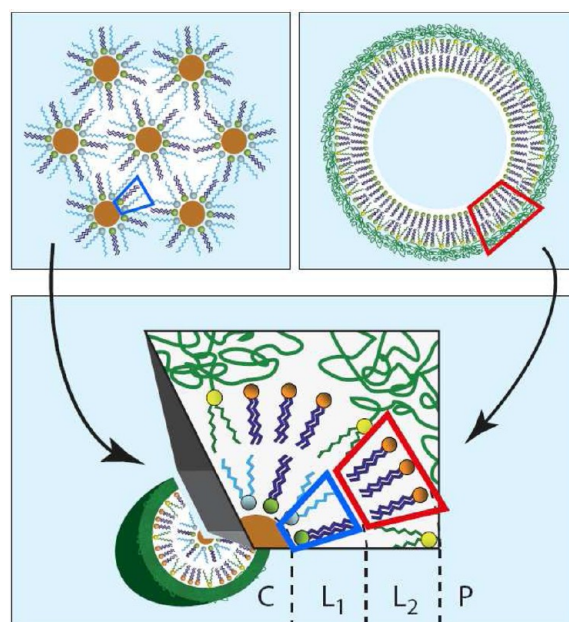


Figure 1. Schematic drawing of the rational design of mono-NALPs: The inner monolayer of the inverted H_{II}^C cationic lipid–DNA phase consisting of the lipid composition DOTAP/DOPE (L1) and the outer monolayer of stealth-liposomes consisting of DOPC/DSPE-PEG(2000) (L2) are combined to encapsulate short ds-DNA. The resulting mono-NALP consists of a DNA core (C), a strongly curved asymmetric lipid bilayer (L1/L2), and a PEG shield (P).

Additionally, PEG shields and sterically stabilizes the mono-NALP against aggregation. A passivation of the particles in this manner is also advantageous for potential targeted gene delivery applications.

2.2. Development of the Assembly Route of mono-NALPs. We study the self-assembly of lipids and DNA for the first time in alcohol mixtures using fluorescence correlation spectroscopy (FCS); see Figure 2a and the Experimental Section for a brief description. We choose 20 base pair double-stranded, Cy5-labeled DNA as a physicochemical model system for siRNA. DNA is less prone to degradation and thus a more eligible experimental tool than siRNA. In a first set of experiments, we investigate the influence of solvent exchange, charge ratio, and PEGylation on the complexation of lipids and ds-DNA. In the end of this section, we demonstrate that the same physicochemical behavior is valid for siRNA. The molar ratios of the lipids are chosen according to the rational design considerations presented in the previous section. DOTAP and DOPE form a lipid monolayer around DNA at molar ratios between 1:3 and 1:5.⁵ To form a lipid bilayer around DNA, we need to add DOPC for the outer monolayer at a molar ratio such that the same amount of DOPC is used as DOTAP and DOPE. Furthermore, to furnish the mono-NALP with the stealth property, a small amount of DSPE-PEG(2000) is added to the lipid mixture. Therefore, we used the final lipid compositions DOTAP:DOPE:DOPC:DSPE-PEG(2000) = 1:3:4:0.8 and 1:5:6:1.2 (molar ratios). For both lipid compositions, we observed the same complexation behavior. Figure 2b shows the formation of particles as a function of increasing water volume percentage in the isopropanol/water solvent. Measurements are done with samples of increasing water content, starting from 40% (v/v). FCS correlation functions yield the particle diffusion time τ_D and the

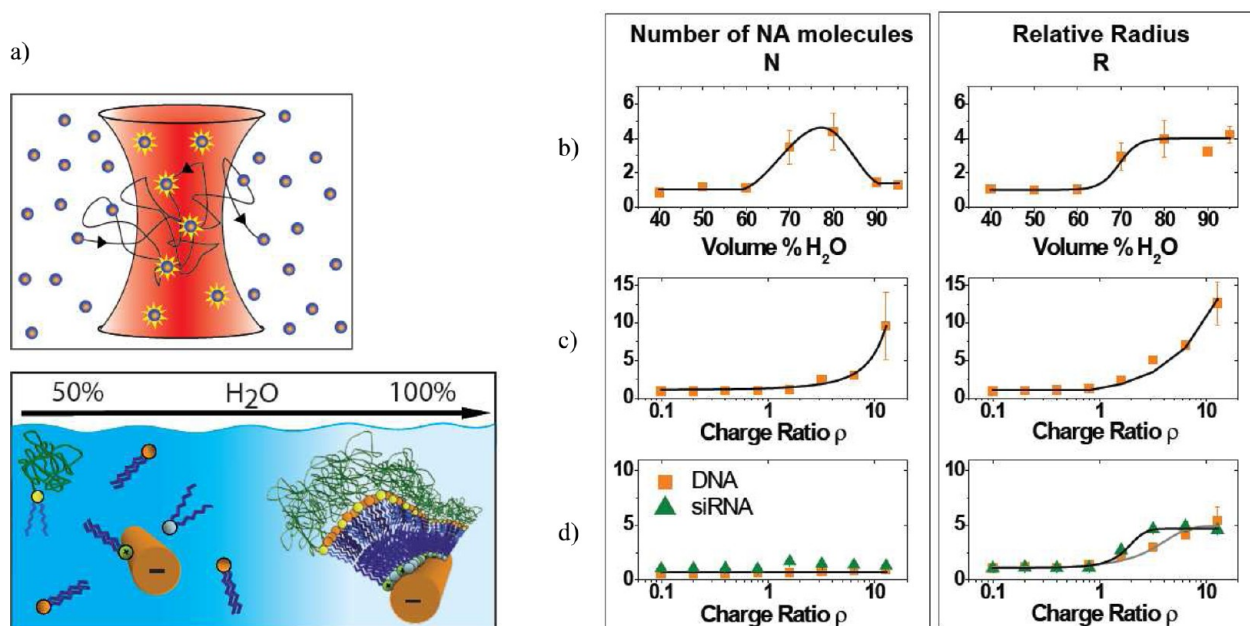


Figure 2. Mono-NALP assembly route. (a) Using fluorescence correlation spectroscopy, the number of fluorescently labeled 20bp ds-DNA molecules per particle N and the relative hydrodynamic particle radius R are measured in isopropanol/water mixtures. (b) A 60% isopropanol/40% water solution containing DNA and lipids (DOTAP:DOPE:DOPC:DSPE-PEG(2000) = 1:5:6:1.2, $\rho = 3.2$) is stepwise diluted in purified water. Reaching 100% water content, mono-NALPs are formed that exhibit a hydrodynamic radius of 16 nm, which is 4 times larger than the naked DNA molecules ($R = 4$). (c,d) The DNA content and the particle size as a function of the cationic lipid–DNA charge ratio ρ in case of lipid mixtures without PEG shielding (c) and with PEG shielding (d). Without the addition of DSPE-PEG(2000), complexes contain several DNA molecules ($N > 1$ for $\rho > 1$) and grow larger ($R > 13$ for $\rho > 10$). In case of PEG-stabilized lipid mixtures, the complexes contain a single DNA or siRNA molecule ($N = 1$ for all compositions) and have maximal hydrodynamic radii of about 20 and 18 nm ($R = 5$ and 4.5), respectively. There is no fundamental difference in the assembly of mono-NALPs based on siRNA as compared to ds-DNA. Solid lines were drawn to guide the eye.

fluorescence intensity per molecule; see the Experimental Section for further details. We normalize both quantities with respect to naked double-stranded oligonucleotides under identical solvent conditions and use the relative diffusion time as a measure for the relative hydrodynamic radius of the particles. In the right column of Figure 2, we show relative hydrodynamic radii R , whereas in the left column the number of double-stranded oligonucleotides per detected fluorescent particle N is estimated from the fluorescence intensity. Up to a concentration of 60% water, DNA molecules remain monomolecular ($N = 1$) at a constant relative size ($R = 1$), meaning that no lipids bind to the DNA. In the intermediate range of 70%–80% water, polydisperse solutions of lipid aggregates containing several DNA molecules ($N > 4$, $R > 2$) exist. This is a sign of the complex phase transitions that lipid mixtures undergo when the solvent is exchanged from isopropanol to water.³² Upon dilution to at least 90% water, mono-NALPs form that include a single DNA molecule ($N = 1$) and have a four times larger hydrodynamic radius ($R = 4$). The hydrodynamic radius of Cy5-labeled 20 base pair ds-DNA is about 4 nm, so these particles have a radius of about 16 nm. This matches the expected size of a micelle-like particle composed of a DNA core (radius 4 nm), a lipid bilayer (thickness 4 nm), and a PEG coating (height 8 nm) as schematically drawn in Figure 1.

Next, we investigate the question to what extent the complexation process depends on the lipid–nucleic acid charge ratio ρ . FCS measurements detect no association of lipids (DOTAP:DOPE:DOPC = 1:5:6) with DNA for charge ratios $\rho < 1$; see Figure 2c. In contrast, beyond the isoelectric point, lipids and ds-DNA aggregate as indicated by the continuous

increase of both the number of DNA per particle N and the relative size of the particles R . Note that in this case the stabilizing DSPE-PEG(2000) is absent: Particles form that contain more than one DNA molecule ($N > 1$) and have relative sizes $R > 5$ for charge ratios ρ greater than 3. For high charge ratios ($\rho > 12$), the FCS correlation function exhibits signatures of aggregates as seen here from the fact that the size distribution becomes considerably broader ($\sim 20\%$) as well as the number distribution of incorporated DNA molecules ($\sim 45\%$).

Remarkably, addition of DSPE-PEG(2000) to the lipid composition completely impedes particle aggregation. Figure 2d shows FCS measurements of DNA and DOTAP:DOPE:DOPC:DSPE-PEG(2000) = 1:5:6:1.2. Even at high lipid–nucleic acid charge ratios ($\rho = 12$), particles show a saturation of the relative particle size at $R = 5$ (20 nm). In particular, for all charge ratios ρ , only particles containing one molecule of nucleic acid are observed. In Figure 2d, we also show the self-assembly using siRNA instead of ds-DNA under identical conditions. The siRNA content and relative particle size of siRNA mono-NALPs follow a trend similar to that in the case of ds-DNA. Depending on the charge ratio ρ , particles containing siRNA have sizes up to $R = 4.5$ (18 nm). Here, the maximum size is already reached at the charge ratio $\rho = 3$, whereas for DNA mono-NALPs a continuous increase of the relative radius is observed for charge ratios up to $\rho = 6.5$.

2.3. Structure of mono-NALPs. To substantiate our picture of the mono-NALP structure, we performed small-angle neutron scattering (SANS), small-angle X-ray scattering (SAXS), and transmission electron microscopy (TEM) experiments.

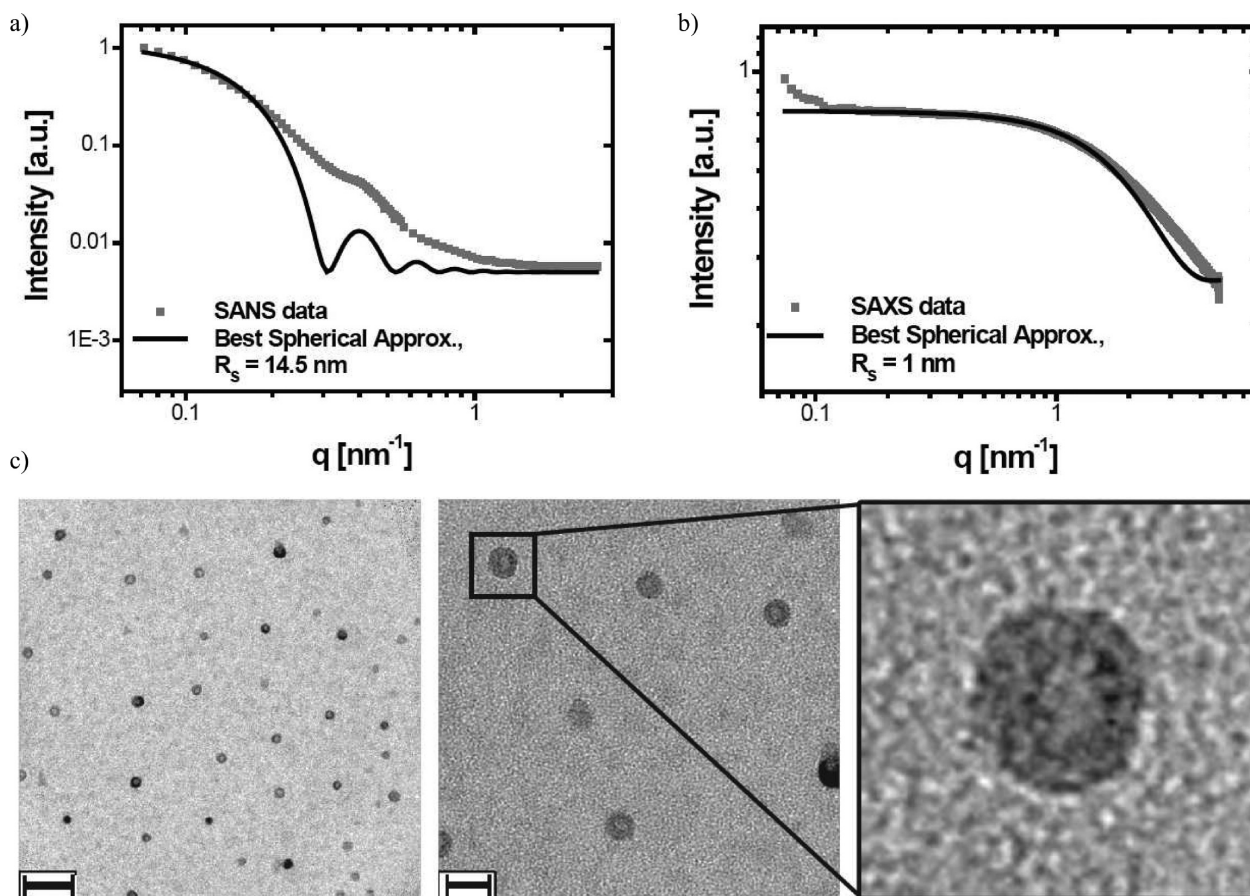


Figure 3. SANS data of (a) mono-NALPs comprised of DNA and DOTAP:DOPE:DOPC:DSPE-PEG(2000) = 1:5:6:1.2 ($\rho = 3.2$) in deuterium. The solid line indicates the theoretical scattering profile of a solid sphere with a radius of 14.5 nm as a reference. The SAXS signal (b) is dominated by the DNA core, whereas SANS data arise from scattering of the entire mono-NALP including the lipid and PEG layer. TEM micrographs (c) show a monodisperse distribution of mono-NALPs (DNA and DOTAP:DOPE:DOPC:DSPE-PEG(2000) = 1:3:4:0.8, $\rho = 3.2$) stained with osmium tetroxide. Scale bars are 90 and 30 nm, respectively. On the right: Magnification of the framed image region showing an apparent particle radius of about 10 nm.

Samples for SANS measurements contained mono-NALPs consisting of 20 base pair ds-DNA and lipids (DOTAP:DOPE:DOPC:DSPE-PEG(2000) = 1:5:6:1.2, $\rho = 3.2$) and were prepared in deuterium oxide (D_2O) to enhance the scattering contrast for neutrons. X-ray samples were likewise prepared in D_2O to ensure comparability. Data were collected at the instrument KWS-2 at the Juelich Centre for Neutron Science, FRM II Munich, and ID2 at the ESRF in Grenoble as described in the Experimental Section. Figure 3a shows a logarithmic intensity plot of the SANS data. The solid line indicates the theoretical scattering profile of a solid sphere of 14.5 nm radius, which is not yet convoluted with the resolution function. The SANS data are in reasonable agreement with the expected, approximately spherical shape and size of mono-NALPs, which in turn is close to the conception of a PEG shielded lipid bilayer coating a 20 base pair ds-DNA molecule. Most importantly, the SANS radius compares favorably with the hydrodynamic radius of about 16 nm measured by FCS. The SAXS signal depicted in Figure 3b, in contrast, is dominated by the high electron density of the DNA phosphate groups in the center of the mono-NALPs and reveals a highly scattering core. To guide the eye, the theoretical scattering curve of a sphere with 2 nm diameter is shown in the plot. The spherical formfactor is a first, crude approximation and does not match the SAXS data well. However, the SAXS data clearly reveal the existence of a

nanometer-ranged scattering core and the absence of Bragg peaks as would be characteristic for ordinary lipid–DNA complexes. In addition, both SAXS and SANS exclude the prevalence of aggregates that would show distinct small-angle scattering.

Transmission electron micrographs of mono-NALPs show monodisperse, ring-like objects with an apparent radius of about 10 nm, as seen in the images and the zoom in Figure 3c. Here, it should be noted that the negative staining procedure using osmium tetroxide selectively stains unsaturated lipids,³³ while the PEG shield of the particles and the DNA core is not visible. Hence, we assume that the ringlike structures correspond to the asymmetric lipid bilayers of the mono-NALPs. The apparent particle radius is slightly larger than expected for a bilayer-coated 20 base pair ds-DNA molecule (6–8 nm, depending on the orientation). This increase in size is most likely caused by the flattening of the originally approximately spherical mono-NALPs on the surface of the TEM grid during sample preparation, which requires complete dehydration (see the Experimental Section). More important than the particles having the expected radius is the observation that all objects found in TEM micrographs are monodisperse and exhibit no indication of aggregation as shown by images of different scale.

2.4. Stability of mono-NALPs. Next, we investigate the steric stability of the core–shell structured mono-NALPs in collagen networks of three different concentrations (0.01, 0.2, and 2.5 mg/mL), the major constituent of the extra cellular matrix.

FCS data are shown in Figure 4a as a function of normalized time τ/η that is used to account for the change of solution

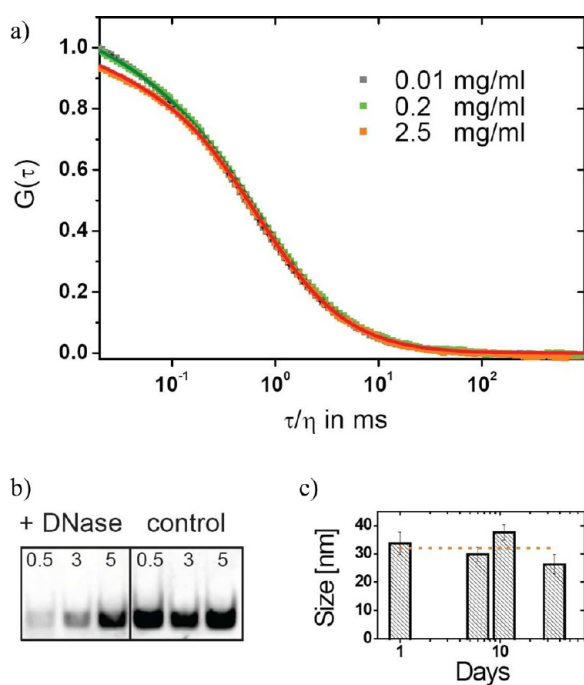


Figure 4. Stability of mono-NALPs. (a) Normalized FCS autocorrelation functions of mono-NALPs show no dependence on collagen concentrations. The time axis is normalized to the solution viscosity. Red and dark green lines represent theoretical fits for freely diffusing particles and overlap perfectly with the data. (b) DNase type I assay: PAGE of DNA recovered from mono-NALPs ($\rho = 0.5, 3, 5$) after incubation with DNase (left) and without DNase (right). (c) Long-term stability of the size of mono-NALPs over several days.

viscosity η with collagen concentration; see the Experimental Section for further detail. The viscosity normalized autocorrelation curves show that the hydrodynamic properties of mono-NALPs are independent of the collagen concentration and hence indicate integrity of the particles. In particular, there are no additional contributions of aggregates in the FCS signal. Furthermore, if the particles would interact with collagen, we would expect a systematic reduction of the diffusion beyond the viscosity effect. Hence, the particles do not bind to collagen nor do they disassemble. Additionally, the nucleic acid within a mono-NALP is effectively protected against degradation by nucleases. Samples of particles composed from DNA and DOTAP:DOPE:DOPC:DSPE-PEG(2000) = 1:5:6:1.2 with three different charge ratios $\rho = 0.5, 3,$ and 5 were exposed to DNase type I for 0.5 h, before the DNA was purified and loaded on a polyacrylamide gel. Results of the gel electrophoresis can be seen in Figure 4b. Almost the entire DNA encapsulated in mono-NALPs with $\rho = 5$ resisted the treatment with DNase. Particles with $\rho = 3$ were partially degraded in agreement with the partial lipid coating measured by FCS at this charge ratio; compare to Figure 2d. FCS measurements performed 1, 6, 11, and 35 days after sample preparation reveal the long-term stability of mono-NALPs: The particle size

deviates within the experimental error and does not systematically increase or decrease over time; see Figure 4c.

2.5. Pegylation Prevents mono-NALPs from Non-specific Binding to Cells. PEGylation does not only prevent particle aggregation but also inhibits the binding of mono-NALPs to cell surfaces. Figure 5a shows a fluorescence

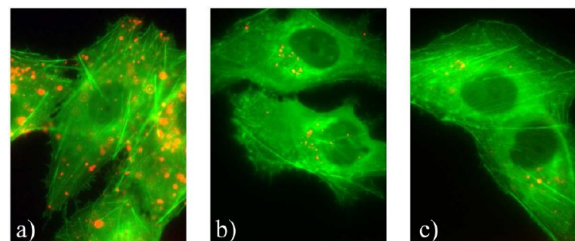


Figure 5. Fluorescence micrographs of GFP-actin expressing HuH-7 cells incubated for 2 h with mono-NALPs (red channel). (a) Particles without PEG, (b) mono-NALPs including DSPE-PEG(2000), and (c) control without mono-NALPs showing some autofluorescence in the red channel. The PEG shielding inhibits nonspecific binding of DNA lipid particles to cells.

microscopy image of cells incubated for 2 h with a 20 nM solution of nucleic acid particles without PEG shielding (DOTAP:DOPE:DOPC = 1:3:4). Aggregates of the particles are visible as red spots, as each DNA molecule carries a Cy5-label. In contrast, no particles can be found on the cell surfaces applying mono-NALPs that are shielded by DSPE-PEG(2000) (DOTAP:DOPE:DOPC:DSPE-PEG(2000) = 1:3:4:0.8), as is shown in Figure 5b). The remaining red spots are caused by autofluorescent cell components, which are also visible in a reference micrograph of untreated cells, Figure 5c. Thus, PEG shielding significantly reduces nonspecific binding of mono-NALPs to cells. This might decrease the potential gene silencing efficacy but enables further functionalization of the particle surface for targeted gene delivery.

3. CONCLUSIONS

We reported on mono-NALPs, the smallest PEGylated and lipid bilayer-coated siRNA particles existing so far. Following rational design principles, we found a self-assembly strategy for the complexation of single nucleic acid molecules with an enveloping asymmetric lipid bilayer and a polymeric PEG shield. The complexation method is easy to reproduce and scale up as mono-NALP formation initiates upon a simple solvent exchange from 50% isopropanol to water by sample dilution. We studied the self-assembly of the particles by FCS and confirmed their core–shell like structure by SANS, SAXS, and TEM. The mono-NALP design assures efficient protection of the DNA from degradation by proteins (DNase type I) as well as a high steric stability, impeding particle aggregation, disassembly in protein networks (collagen), and nonspecific binding to cells. Hence, the mono-NALP represents a well-defined and highly stabilized siRNA carrier, albeit nonadhering to cells and hence inactive. Clearly, the next steps toward the design of an effective carrier system are the implementations of specific targeting and intracellular release mechanisms, for example, via pH-sensitive linker chemistry.²³ However, we would like to stress that the mono-NALP design is the groundwork for specific targeting that requires low nonspecific binding *in vivo*. In addition, the small diameter of the particles (approximately 30 nm) should facilitate their transport *in vivo*

for example in inflamed tissue or solid tumors.¹⁸ Because of their stable physical-chemical properties and a long shelf life, we believe that the mono-NALP design and self-assembly route can serve as a fundament for the development of novel gene delivery systems with enhanced in vivo efficacy.

4. EXPERIMENTAL SECTION

Materials. Lipids (DOTAP 1,2-dioleoyl-3-trimethylammonium-propane, DOPE 1,2-dioleoyl-*sn*-glycero-3-phosphoethanolamine, DOPC 1,2-dioleoyl-*sn*-glycero-3-phosphocholine, and DSPE-PEG(2000) 1,2-distearoyl-*sn*-glycero-3-phosphoethanolamine-*N*-[(polyethylene glycol)-2000]) were purchased from Otto Nordwald GmbH, Hamburg, Germany, a distributor of Avanti Polar Lipids Inc., Alabaster, AL, and used without further purification. Single-stranded DNA oligonucleotides were ordered in lyophilized form from metabion international AG, Planegg-Martinsried, Germany. Two complementary sequences of 20 bases were used: 5'-GCA-AGC-TGA-CCC-TGA-AGT-TC-3' and 5'-GAA-CTT-CAG-GGT-CAG-CTT-GC-3'. For FCS experiments and fluorescence microscopy, the 5'-end of one of the single strands was modified by a covalently bound Cy5-molecule. Collagen type I solution from rat tail was purchased from Sigma-Aldrich Chemie GmbH, Munich, Germany, and used without further treatment. Rotiphorese Gel 30 and TEMED 99% for polyacrylamide gel electrophoresis were obtained from Carl Roth GmbH & Co. KG, Karlsruhe, Germany; SYBR gold nucleic acid gel stain was purchased from Invitrogen, Karlsruhe, Germany.

Instrumentation. FCS experiments were conducted on an Axiovert 200 microscope with a ConfoCor 2 unit (Carl Zeiss, Jena, Germany), equipped with a 40× (1.2 NA) water immersion apochromatic lens (Carl Zeiss Jena, Germany). A HeNe laser (633 nm, 5 mW) provided the excitation that was separated from fluorescence emission by a 650 nm long pass filter. For measurement, samples were contained in eight-well LabTek I chamber slides (nunc, Wiesbaden, Germany). The ConfoCor 2 software was used for autocorrelation and analysis of the intensity signal. TEM micrographs were taken with a JEM-1011 transmission electron microscope (JEOL, Tokyo, Japan) at 100 kV. Fluorescence microscopy was performed on a Simple PCI (Compix) controlled motorized inverted microscope with an oil-immersion objective (100× magnification, 1.3 NA). A Nikon Intensilight HG Precentered Fiber Illumination system was used as light source together with two different filter blocks: EGFP was detected using the filter set BP450-490, FT510, BP510-565, and Cy5 was detected using the set BP608-648, FT660, BP652-732. The detector was a CoolSNAP HQ monochrome camera. Images were acquired with an oil-immersion objective.

Preparation of Lipid Solutions and mono-NALPs. For all experiments presented in this Article, lipid compositions of DOTAP:DOPE:DOPC:DSPE-PEG(2000) with fixed molar ratios of 1:3:4:0.8 or 1:5:6:1.2 were used, unless otherwise noted. To prepare lipid stock solutions, required amounts of lipids, dissolved in chloroform or as powder, are given into a clean vial and dried under nitrogen if necessary. Residual chloroform is removed by vacuum-drying overnight at room temperature. The lipids are resolved in 50% isopropanol/water and stored at 4 °C. The solutions are sonicated with a tip sonicator for at least 30 s each time before use. For the preparation of mono-NALPs, according volumes of lipid stock solutions and siRNA or DNA (in PBS) are pipetted into a vial or tube containing isopropanol and purified water, such that the final solvent consists of 50% isopropanol/water. The solution is well shaken, diluted 10 times in purified water to generate mono-NALPs, and again well but carefully mixed on a vortex mixer. To increase the sample concentration without loss of material, the solutions can be placed in a vacuum oven or a vacuum centrifuge at 40 °C until sufficient reduction in volume is achieved. Alternatively to purified water, the particles can be prepared in PBS.

Fluorescence Correlation Spectroscopy. Fluorescence correlation spectroscopy has become an established technique,³⁴ whereof only a brief description will follow. Using a confocal microscope and a laser, the fluctuating fluorescence signal of a low concentrated

fluorophore solution is recorded; see Figure 2a. The time-dependent autocorrelation of the measured intensity profile is in the simplest case described by

$$G(\tau) = 1 + \frac{1}{n} \left(1 + \frac{\tau}{\tau_D} \right)^{-1} \left(1 + \frac{\tau}{S^2 \tau_D} \right)^{-1/2} \quad (1)$$

n is the number of fluorophores in the detection volume, the diffusion time τ_D is inverse proportional to the diffusion constant D of the fluorophores, and S is the form factor of the detection volume. The hydrodynamic radius R_h of a spherical particle is related to its diffusion constant via the Stokes–Einstein relation:

$$R_h = \frac{k_B T}{6\pi\eta D} \quad (2)$$

where η is the solvent viscosity, k_B is the Boltzmann constant, and T is the temperature. Additionally, the number of fluorescently labeled nucleic acid molecules incorporated in a lipid particle can be determined with FCS by comparing the fluorescence intensity of mono-NALPs with that of single labeled DNA or siRNA molecules. Addition of collagen to the solvent slows diffusion in a viscosity-dependent manner and thus effects the measured diffusion time. Also, in contrast to measurements performed in isopropanol/water solutions, the particle size cannot be determined by direct comparison to diffusion times obtained from pure DNA or siRNA samples as nucleic acids aggregate with positively charged proteins. Instead, to gain information about changes in particle size, the measured autocorrelation curves need to be normalized to the viscosity of the collagen solution. The viscosity of a polymer solution η_p depends on its concentration C_p :^{35,36}

$$\frac{\eta_p}{\eta_s} = 1 + \frac{C_p}{C^*} + k_H \left(\frac{C_p}{C^*} \right)^2 \quad (3)$$

where η_s denotes the solvent viscosity, C^* is the polymer overlap concentration, and k_H is the Huggins coefficient. Collagen has an overlap concentration of 2.7 mg/mL,³⁷ and the Huggins coefficient is estimated to be $k_H \approx 0.6$.³⁸

Preparation of Samples for Transmission Electron Microscopy. Mono-NALPs are freshly prepared as described above. About 10 μ L of sample solution is given on a Formvar-carbon copper grid, and about 5 μ L of an aqueous osmium tetroxide solution (4%) is added. After 30 s, the grid is plunged into liquid nitrogen to rapidly freeze the sample before it is lyophilized. Dry grids are stored at room temperature until use.

Small-Angle Neutron Scattering. Neutron experiments were carried out at the KWS2 SANS diffractometer of the Juelich Center of Neutron Science (JCNS) hosted at the FRMII research reactor in Garching.³⁹ The experiments were performed with neutrons of wavelength of 7 Å with a 20% half width of maximum, 2 and 8 m at sample-to-detector distances to adjust the right wave vector interval. The obtained scattering data were corrected for background scattering and sensitivity of the individual detector channels, and finally evaluated in absolute units by calibration with Plexiglas secondary standard (qtiKWS software package).⁴⁰

Small-Angle X-ray Scattering. SAXS experiments were carried out at the beamline ID02 at the ESRF (Grenoble). Samples were prepared as described for the neutron experiments to ensure comparability of the scattering data. 2 mm quartz capillaries were used as sample holders, and background correction was carried out for each scan individually by subtracting the scattering signal of a water-filled capillary adjusted by a factor accounting for the variation in the capillary diameters.

DNase-Assay. Mono-NALPs are prepared whereof 25 μ L (containing 0.5 μ g of DNA) is given into a microcentrifuge tube, together with 50 μ L of a 10 mM MgCl₂/5 mM CaCl₂ solution and 5 μ L of DNase type I (10 μ g/mL). After incubation for 30 min at room temperature, 75 μ L of stop mix (20 mM EDTA pH 8, 1% w/v SDS, 0.2 M NaCl) is added and the samples are stored at 4 °C. Purification of DNA from the samples was done as follows: To each sample were

added 400 μL of 100% ethanol ($-20\text{ }^\circ\text{C}$) and 10 μL of NaAc solution (3 M), then they were vortexed and plunged into liquid nitrogen. After 2 min, the microcentrifuge tubes were centrifuged for 10 min at $4\text{ }^\circ\text{C}$ to sediment the remaining DNA. The solvent was carefully removed, 500 μL of 70% ethanol was refilled, and the tubes were centrifuged again (5 min, $4\text{ }^\circ\text{C}$) before the ethanol was removed. Finally, the sample tubes were dried under vacuum. The purified DNA (resolved in PBS) can be analyzed by polyacrylamide gel electrophoresis (PAGE).

Cell Line and Cell Culture. We use HuH-7 human hepatoma cells (JCRB 0403; Tokyo, Japan; cell diameters up to 70 μm) stably expressing EGFP-actin. Cells are grown in Dulbecco's modified Eagle's medium:F12 (1:1) with 5 mM L-glutamine containing 10% fetal bovine serum at $37\text{ }^\circ\text{C}$ in a humidified atmosphere, 5% CO_2 level. Cells are maintained at 85% confluence, trypsinized, washed with PBS, resuspended in DMEM (10% FBS and 5 mM L-glutamine), and counted using a Neubauer counting chamber.

Cell Binding Study. Cells are resuspended in DMEM (10% FBS and 5 mM L-glutamine) to achieve a concentration of 105 cells/mL. Thirty microliters of this cell suspension is added to each channel in μ -slides VI. After 10 min, enough medium is added to fill the reservoirs. Cells are incubated overnight at $37\text{ }^\circ\text{C}$ in a humidified atmosphere, 5% CO_2 level. Channels are rinsed once with PBS and once with fresh medium, before they are refilled with medium containing 20 nM of Cy5-labeled mono-NALPs. After 2 h, the channels are again rinsed, once with PBS and once with CO_2 -independent medium, L-15 (10% FBS and 5 mM L-glutamine), before refilling them with L-15. Thereafter, fluorescence images are immediately taken.

AUTHOR INFORMATION

Corresponding Author

joachim.raedler@lmu.de

Present Address

[†]Max-Planck-Institute of Colloids and Interfaces, Science Park Golm, D-14476 Potsdam, Germany.

Notes

The authors declare no competing financial interest.

ACKNOWLEDGMENTS

We thank Manfred Ogris for the kind gift of EGFP-actin expressing HuH-7 human hepatoma cells and Sylvio May for helpful discussions on theoretical aspects of the particle formation process. We thank Peter Busch, Vitaliy Pipich (FRM-II), and Theyencheri Narayanan (ESRF) and Jennifer McManus for technical assistance at the SANS and SAXS beamlines, respectively. Financial support by the German Excellence Initiative of the Deutsche Forschungsgemeinschaft through the "Nanosystems Initiative Munich" Research Cluster is gratefully acknowledged.

REFERENCES

- (1) Felgner, P. L.; Gadek, T. R.; Holm, M.; Roman, R.; Chan, H. W.; Wenz, M.; Northrop, J. P.; Ringold, G. M.; Danielsen, M. *Proc. Natl. Acad. Sci. U.S.A.* **1987**, *84*, 7413.
- (2) Zhang, S. B.; Zhao, B.; Jiang, H. M.; Wang, B.; Ma, B. C. *J. Controlled Release* **2007**, *123*, 1.
- (3) Radler, J. O.; Koltover, I.; Salditt, T.; Safinya, C. R. *Science* **1997**, *275*, 810.
- (4) Lasic, D. D.; Strey, H.; Stuart, M. C. A.; Podgornik, R.; Frederik, P. M. *J. Am. Chem. Soc.* **1997**, *119*, 832.
- (5) Safinya, C. R. *Curr. Opin. Struct. Biol.* **2001**, *11*, 440.
- (6) Li, W. J.; Szoka, F. C. *Pharm. Res.* **2007**, *24*, 438.
- (7) Dorsett, Y.; Tuschl, T. *Nat. Rev. Drug Discovery* **2004**, *3*, 318.
- (8) de Fougères, A.; Vornlocher, H. P.; Maraganore, J.; Lieberman, J. *Nat. Rev. Drug Discovery* **2007**, *6*, 443.

- (9) Hayes, M. E.; Drummond, D. C.; Kirpotin, D. B.; Zheng, W. W.; Noble, C. O.; Park, J. W.; Marks, J. D.; Benz, C. C.; Hong, K. *Gene Ther.* **2006**, *13*, 646.

- (10) Hayes, M. E.; Drummond, D. C.; Hong, K.; Park, J. W.; Marks, J. D.; Kirpotin, D. B. *Biochim. Biophys. Acta, Biomembr.* **2006**, *1758*, 429.

- (11) Jeffs, L. B.; Palmer, L. R.; Ambegia, E. G.; Giesbrecht, C.; Ewanick, S.; MacLachlan, I. *Pharm. Res.* **2005**, *22*, 362.

- (12) Morrissey, D. V.; Lockridge, J. A.; Shaw, L.; Blanchard, K.; Jensen, K.; Breen, W.; Hartsough, K.; Machemer, L.; Radka, S.; Jadhav, V.; Vaish, N.; Zinnen, S.; Vargeese, C.; Bowman, K.; Shaffer, C. S.; Jeffs, L. B.; Judge, A.; MacLachlan, I.; Polisky, B. *Nat. Biotechnol.* **2005**, *23*, 1002.

- (13) Akinc, A.; Zumbuehl, A.; Goldberg, M.; Leshchiner, E. S.; Busini, V.; Hossain, N.; Bacallado, S. A.; Nguyen, D. N.; Fuller, J.; Alvarez, R.; Borodovsky, A.; Borland, T.; Constien, R.; de Fougères, A.; Dorkin, J. R.; Jayaprakash, K. N.; Jayaraman, M.; John, M.; Kotliarsky, V.; Manoharan, M.; Nechev, L.; Qin, J.; Racie, T.; Raitcheva, D.; Rajeev, K. G.; Sah, D. W. Y.; Soutschek, J.; Toudjarska, I.; Vornlocher, H. P.; Zimmermann, T. S.; Langer, R.; Anderson, D. G. *Nat. Biotechnol.* **2008**, *26*, 561.

- (14) Akinc, A.; Goldberg, M.; Qin, J.; Dorkin, J. R.; Gamba-Vitalo, C.; Maier, M.; Jayaprakash, K. N.; Jayaraman, M.; Rajeev, K. G.; Manoharan, M.; Kotliarsky, V.; Rohl, I.; Leshchiner, E. S.; Langer, R.; Anderson, D. G. *Mol. Ther.* **2009**, *17*, 872.

- (15) Leal, C.; Ewert, K. K.; Shirazi, R. S.; Boussein, N. F.; Safinya, C. R. *Langmuir* **2011**, *27*, 7691.

- (16) Leal, C.; Boussein, N. F.; Ewert, K. K.; Safinya, C. R. *J. Am. Chem. Soc.* **2010**, *132*, 16841.

- (17) Whitehead, K. A.; Langer, R.; Anderson, D. G. *Nat. Rev. Drug Discovery* **2009**, *8*, 516.

- (18) Maeda, H. *Adv. Enzyme Regul.* **2001**, *41*, 189.

- (19) Gao, K. P.; Jiang, X. G. *Int. J. Pharm.* **2006**, *310*, 213.

- (20) Blessing, T.; Remy, J. S.; Behr, J. P. *Proc. Natl. Acad. Sci. U.S.A.* **1998**, *95*, 1427.

- (21) Chittimalla, C.; Zammuto-Italiano, L.; Zuber, G.; Behr, J. P. *J. Am. Chem. Soc.* **2005**, *127*, 11436.

- (22) DeRouchey, J.; Walker, G. F.; Wagner, E.; Radler, J. O. *J. Phys. Chem. B* **2006**, *110*, 4548.

- (23) DeRouchey, J.; Schmidt, C.; Walker, G. F.; Koch, C.; Plank, C.; Wagner, E.; Radler, J. O. *Biomacromolecules* **2008**, *9*, 724.

- (24) Sternberg, B.; Sorgi, F. L.; Huang, L. *FEBS Lett.* **1994**, *356*, 361.

- (25) Sternberg, B. *J. Liposome Res.* **1996**, *6*, 515.

- (26) May, S.; BenShaul, A. *Biophys. J.* **1997**, *73*, 2427.

- (27) Tresset, G.; Lansac, Y.; Romet-Lemonne, G. *Langmuir* **2012**, *28*, 5743.

- (28) Raviv, U.; Needleman, D. J.; Li, Y. L.; Miller, H. P.; Wilson, L.; Safinya, C. R. *Proc. Natl. Acad. Sci. U.S.A.* **2005**, *102*, 11167.

- (29) Koltover, I.; Salditt, T.; Radler, J. O.; Safinya, C. R. *Science* **1998**, *281*, 78.

- (30) Zimmerberg, J.; Kozlov, M. M. *Nat. Rev. Mol. Cell Biol.* **2006**, *7*, 9.

- (31) Johansson, M.; Hansson, P.; Edwards, K. *J. Phys. Chem. B* **2001**, *105*, 8420.

- (32) Hohner, A. O.; David, M. P. C.; Radler, J. O. *Biointerphases* **2010**, *5*, 1.

- (33) Hayes, T. L.; Gofman, J. W.; Lindgren, F. T. *J. Cell Biol.* **1963**, *19*, 251.

- (34) Hausteiner, E.; Schwill, P. *Annu. Rev. Biophys. Biomol. Struct.* **2007**, *36*, 151.

- (35) Davidson, N. S.; Fetters, L. J.; Funk, W. G.; Hadjichristidis, N.; Graessley, W. W. *Macromolecules* **1987**, *20*, 2614.

- (36) Gold, D.; Onyememezu, C.; Miller, W. G. *Macromolecules* **1996**, *29*, 5700.

- (37) Bueno, E. M.; Ruberti, J. W. *J. Membr. Sci.* **2008**, *321*, 250.

- (38) Sakai, T. *J. Polym. Sci., Part A-2: Polym. Phys.* **1968**, *6*, 1535.

- (39) www.jcns.info.

- (40) www.qtikws.de.